

Splitting of electronic spectrum in paramagnetic phase of itinerant ferromagnets and altermagnets

A. A. Katanin

*Center for Photonics and 2D Materials, Moscow Institute of Physics and Technology,
Institutsky lane 9, Dolgoprudny, 141700, Moscow region, Russia and*

*M. N. Mikheev Institute of Metal Physics of the Ural Branch of the Russian Academy of Sciences,
S. Kovalevskaya Street 18, 620990 Yekaterinburg, Russia*

We study self-energy effects, induced by strong magnetic fluctuations in paramagnetic phase of strongly-correlated itinerant magnets within the density functional theory combined with the dynamical mean field theory (DFT+DMFT approach) and its non-local extension. As concrete examples, we consider α -iron, half metal CrO_2 , van der Waals material CrTe_2 , and altermagnet CrSb . We show that both local and non-local magnetic correlations yield splitting of the electronic spectrum in the paramagnetic phase, such that it closely resembles the DFT band structure in the ordered phase and suppresses spectral weight at the Fermi level. The relative importance of non-local vs. local correlations depends on the proximity to half filling of d states: closer to half filling, the role of local correlations increases. Although the obtained split bands do not possess a certain spin projection, their splitting suppresses spectral weight at the Fermi level. The obtained electronic states are also expected to be easily spin polarized by a weak external magnetic field.

First explanation of itinerant magnetism was given by E. Stoner in 1938 [1] and it was suggested that ferromagnetism in metals is accompanied by splitting of electronic bands due to exchange interaction contribution to the free energy, proportional to the square of magnetization. This contribution was shown to originate from the on-site Coulomb repulsion [2], as it is also described in many textbooks [3–7]. Although in strongly correlated systems correlation effects may in general lead to renormalization of bands, in the ferromagnetically ordered state these effects are suppressed by the band splitting, and therefore Stoner picture remains qualitatively applicable.

The situation is different in the paramagnetic phase even sufficiently close to the magnetic transition. While in two-dimensional systems the so-called quasi-splitting of Fermi surfaces may occur [8–10], in three-dimensional systems the magnetic correlations are generally weaker, and not sufficient to establish a pronounced change of electronic spectrum. At the same time, two effects appear to be important in the paramagnetic phase. The first effect is the presence of local correlations, which originate mainly from Hund interaction in the so-called Hund metals [11–14]. They lead to the formation of local magnetic moments and non-Fermi-liquid behavior and/or non-quasiparticle form of some of the electronic bands. Notably, many “classical” magnets, e.g. iron [15, 16], as well as many other transition metals and their compounds, belong to the class of Hund metals. Although the importance of this effect for quasi-splitting of the Fermi surfaces was discussed previously for the two-orbital model [9], the study of its effect in multi-orbital is of certain interest.

The second effect is the presence in many magnetic systems of the so-called extended van Hove singularities, which represent lines of van Hove singularities and yield strong peaks of the density of states [17]. These singularities effectively reduce the dimension of the system and may lead to stronger renormalization of the electronic

spectrum by the non-local (e.g. magnetic) correlations. In our opinion, the effect of these singularities on the renormalization of the electronic spectrum in the paramagnetic phase was not investigated in detail.

In the present paper we consider the effects of local and non-local contributions to self-energy in several metallic magnets. We consider magnets, belonging to different classes, but all having extended van Hove singularities close to the Fermi level. In particular, we investigate the effects of the self-energy in strong magnet (α -iron), half metal (CrO_2), van der Waals magnet CrTe_2 , and altermagnet CrSb . We show that the effects of the local self-energy are pronounced only very near half filling (which is the case of CrTe_2 and CrSb), while the non-local self-energy effects are pronounced for systems further away from half filling (i.e., for iron and CrO_2). In combination, in all considered systems, these two effects yield splitting of the electronic spectrum near the van Hove singularity, which is strikingly qualitatively similar to that obtained within the DFT calculation in the ferromagnetic phase, although the obtained bands do not possess certain spin orientation.

To describe the effect of local correlations we use the standard DFT+DMFT approach [18–21]. The non-local self-energy effects can be described within the multi-orbital systems the ab initio dynamic vertex approximation (D Γ A) [22–24], which is an extension of the earlier proposed single-band D Γ A [25, 26]. The multi-orbital approach, however, was previously derived for SU(2) symmetry of Hund interaction, the consideration of which is rather computationally time-consuming. We therefore consider its formulation and implementation for Ising symmetry of Hund interaction, which is obtained with the help of the recently proposed unambiguous fluctuation decomposition of the self-energy [27].

General formalism. We consider the DFT+DMFT approach with the tight-binding multiorbital Hubbard

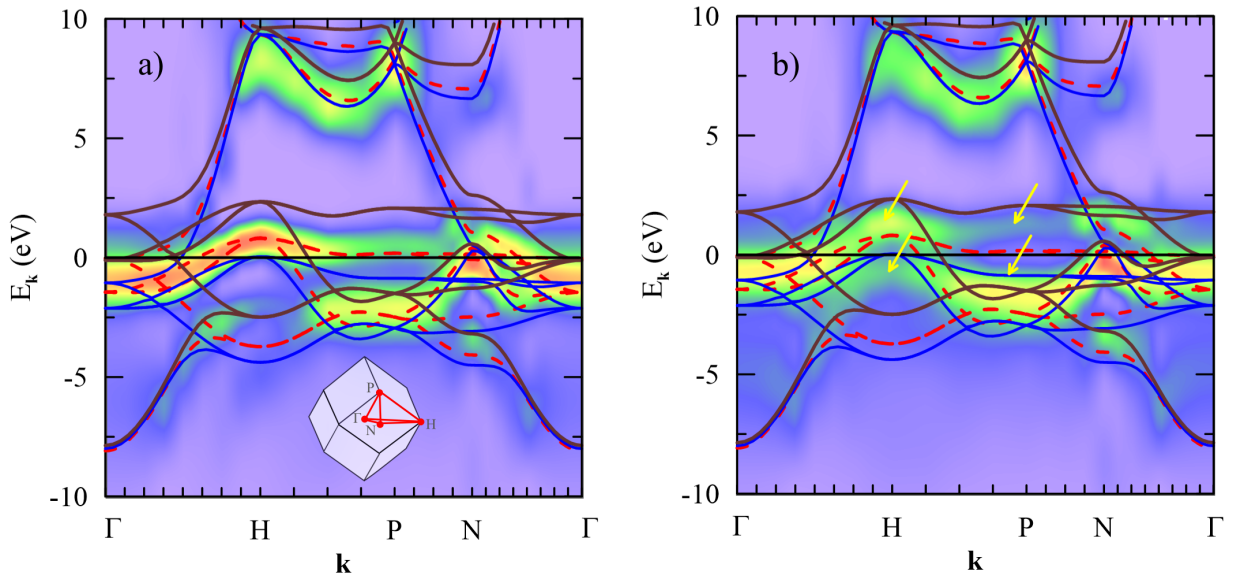


FIG. 1: (Color online) Band structure of iron in the ferromagnetic (brown and blue solid lines for different spin projections) and non-magnetic (red dashed lines) phases, compared to the spectral density in DMFT approach (a) and the approach, accounting for the non-local corrections to the self-energy (b) at $\beta = 4.6 \text{ eV}^{-1}$. Yellow arrows in (b) show position of bands, formed by spin fluctuations in paramagnetic phase. Inset in (a) shows the path in the Brillouin zone.

model

$$H = \sum_{\mathbf{k}, \lambda \lambda', \sigma} H_{\mathbf{k}}^{\lambda \lambda'} c_{\mathbf{k} \lambda \sigma}^{\dagger} c_{\mathbf{k} \lambda' \sigma} + H_{\text{int}} - H_{\text{DC}}, \quad (1)$$

describing electrons which are moving on the sites of the lattice ($c_{\mathbf{k} \lambda \sigma}^{\dagger}$ and $c_{\mathbf{k} \lambda \sigma}$ are the electron creation and destruction operators, λ, λ' are the orbital indices), subject to the on-site Coulomb repulsion H_{int} , and H_{DC} is the double counting contribution, which is needed to keep the ab initio quasiparticle energies, obtained by diagonalizing $H_{\mathbf{k}}^{\lambda \lambda'}$ unchanged by the interaction. For the Coulomb repulsion we consider a density-density Hamiltonian

$$H_{\text{int}} = \frac{1}{2} \sum_{i, m m', \sigma \sigma'} U_{\sigma \sigma'}^{m m'} n_{i m \sigma} n_{i m' \sigma'}, \quad (2)$$

where $n_{i m \sigma} = c_{i m \sigma}^{\dagger} c_{i m \sigma}$ (the indices m, m' numerate d -orbitals). The local self-energy $\Sigma_{\text{loc}, \nu}^m$, obtained within DMFT, is used to obtain the DMFT non-local Green's function $G_{\mathbf{k}}^{m m'} = [i\nu_n + \mu + M_{\text{DC}} - H_{\mathbf{k}} - \Sigma_{\text{loc}, \nu}^m]^{-1}$ where M_{DC} is the double counting contribution to the self-energy and $k = (i\nu_n, \mathbf{k})$ is the frequency and wave vector multi-index.

The non-local self-energy is obtained as (see Supplemental Material [28])

$$\begin{aligned} \Sigma_{\mathbf{k}}^{m m'} &= \Sigma_{\nu}^{\text{loc}, m m'} + \frac{1}{2} T \mathcal{N}_l \sum_{q, \tilde{m}} \left[\gamma_{c, k q}^{m \tilde{m}} W_{c, q}^{\tilde{m} m'} \right. \\ &\quad \left. + 3 \gamma_{s, k q}^{m \tilde{m}} W_{s, q}^{\tilde{m} m'} \right] G_{k+q}^{m m'} \end{aligned} \quad (3)$$

where the first and second terms in the square bracket describe the contribution of charge and spin fluctuations,

$\chi_{k'q}^{0, m' \tilde{m}'} = -T G_{k'}^{m' \tilde{m}'} G_{k'+q}^{\tilde{m}' m'}$ is the bare bubble, $W_{c(s)}^{m m'}$ is the renormalized charge (spin) interaction, and $\gamma_{c(s), k q}^{m \tilde{m}}$ are the triangular Hedin vertices (see Ref. [28]), \mathcal{N}_l means the non-local part of the following expression.

Numerical results. For numerical analysis we consider α -iron, CrO_2 , CrTe_2 and altermagnet CrSb . For DFT calculations we use the Quantum Espresso package [32] with ultrasoft pseudopotentials from the SSSP PBEsol Precision library [33], with subsequent Wannier projection using maximally localized Wannier functions, obtained within the Wannier90 package [34]. The DFT+DMFT approach to study exchange interactions in the three former metallic ferromagnets was considered in Refs. [29–31]. We use the Slater parametrization of Coulomb interaction with around-mean-field form of the double counting correction [35]. For DMFT calculations we use segment continuous time Monte-Carlo (CT-QMC) [36] IQIST solver [37], which allows us to considerably reduce the stochastic noise and obtain the details of the frequency dependence of the vertex functions over a sufficiently broad frequency range. We also use the corrections for finite frequency box in Bethe-Salpeter equations [38]; further details can be found in Refs. [29–31]. The obtained Green's functions, containing local or non-local self-energies, are analytically continued to the real axis using ANA.CONT package [39].

In Fig. 1 we compare the DFT band structures of iron in non-magnetic and ferromagnetic phases with the spectral density in DFT+DMFT approach and the result, accounting for the non-local contributions to the self-energy in Eq. (3). The DMFT approach is applied at $\beta = 1/(k_B T) = 4.6 \text{ eV}^{-1}$ ($T = 2900 \text{ K}$) at $U =$

$F^0 = 4$ eV and Hund exchange $J = 0.9$ eV. Relatively high temperature is chosen in view of high Curie temperature of iron in the density-density approach, which corresponds to $\beta_c = 4.87$ eV $^{-1}$ ($T_C = 2380$ K). The respective uniform susceptibility at the considered temperature $\chi_{\mathbf{q}=0} = 105$ eV $^{-1}$ is much larger than the local transverse susceptibility $\chi_{\text{loc}} = 12$ eV $^{-1}$. One can see (Fig. 1a) that the spectral density in DMFT approach is sufficiently close to the DFT band structure in the non-magnetic phase, with a slight shift of the flat band in the direction H - P - N slightly away from the Fermi level. The non-local effects (see Fig. 1b) yield a stronger shift of this band and a resulting qualitative change of the band structure, which becomes remarkably similar to the DFT band structure in the ferromagnetic phase due to the non-local spin fluctuations. In particular, we

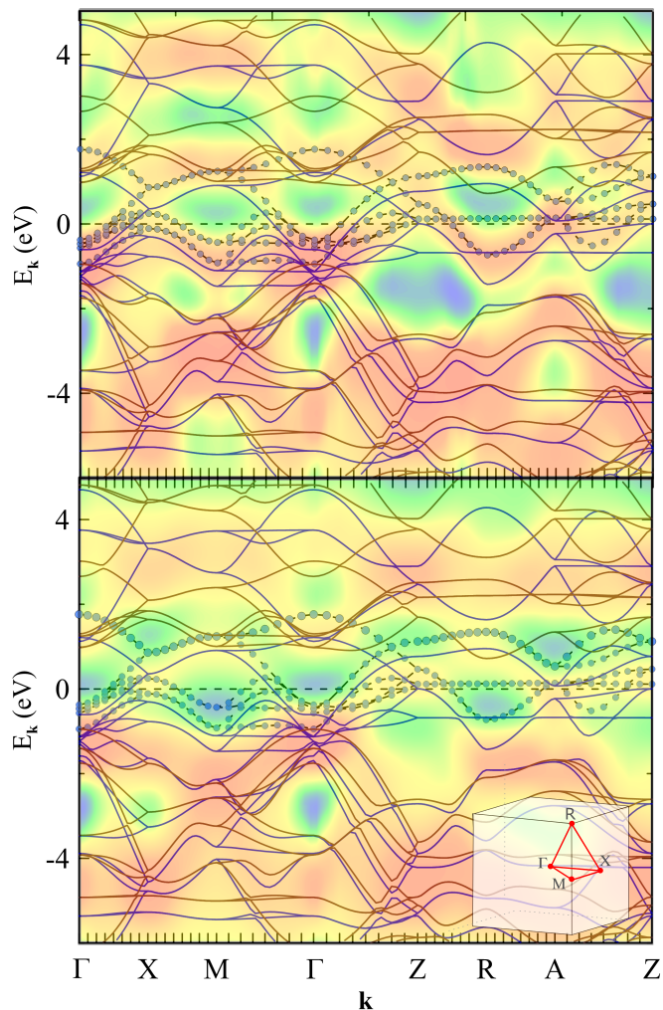


FIG. 2: (Color online) Band structure of CrO $_2$ in the ferromagnetic phase (brown and blue solid lines for different spin projections) and low-energy (mostly d) states in non-magnetic phase (circles) compared to the spectral density in DFT+DMFT approach (top) and the approach, accounting the non-local corrections to the self-energy (bottom) at $\beta = 6$ eV $^{-1}$.

observe splitting of the band structure along the H - P - N direction in momentum space (where the extended van Hove singularity was present). This splitting is reminiscent of the earlier discussed quasi-splitting in the single-band two-dimensional systems [8–10], but it differs from that case by both dimensionality and multi-band electronic structure. We note that the obtained features of electronic structure persist in a wider temperature range, with a continuous shift towards the non-magnetic band structure, see Supplemental Material.

In Fig. 2 we plot the spectral functions of DFT+DMFT and non-local approach to CrO $_2$ at $\beta = 6.5$ eV $^{-1}$ in comparison with the DFT band structures for nonmagnetic and ferromagnetic phases. We use the interaction strength considered previously in Refs. [30, 40], $F^0 = 1.99$ eV, $F^2 = 7.67$ eV, and $F^4 = 5.48$ eV. In the Wannier projection, we include both Cr d and oxygen p states (which results in an 11-orbital model per Cr site, see Ref. [30]), but we have verified that qualitatively similar results are obtained within 5-orbital model, including Cr d states only. The considered temperature is also chosen to be sufficiently close to the DFT+DMFT Curie temperature $\beta_c = 6.8$ eV $^{-1}$ ($T_C = 1700$ K). The respective uniform susceptibility at the considered temperature $\chi_{\mathbf{q}=0} = 110$ eV $^{-1}$ is also much larger than the local susceptibility $\chi_{\text{loc}} = 12$ eV $^{-1}$, and they are qualitatively close to those considered for iron. In case of CrO $_2$, DMFT yields somewhat stronger change of electronic band structure than in iron; in particular it shifts the flat band in the direction Z - R - A away from the Fermi level, which makes the band structure similar to that obtained within DFT for the ordered phase. Considering the effect of the non-local self-energy yields stronger splitting of bands, yielding again qualitative agreement with the ferromagnetic DFT band structure. Stronger effect of the local self-energy in CrO $_2$ in comparison to iron can be attributed to somewhat closer proximity to half filling of d states ($n_d^{\text{CrO}_2} = 3.76$ vs. $n_d^{\text{Fe}} = 6.4$).

In Fig. 3 we present the results for bulk van der Waals magnet CrTe $_2$ at $T = 1600$ K ($\beta = 7.3$ eV $^{-1}$) which is above the magnetic transition temperature $T_c = 950$ K ($\beta_c = 12.2$ eV $^{-1}$; we choose $U = 2.8$ eV, $J = 0.9$ eV). We obtain the maximum of the susceptibility $\chi_{\mathbf{q}A} = 95$ eV $^{-1}$, which corresponds to the tendency of antiferromagnetic ordering between the layers [31], and $\chi_{\text{loc}} = 41$ eV $^{-1}$. In that case, already in DFT+DMFT approach, we find strong band splitting, which originates from the local magnetic correlations. This can be attributed to the relatively large local susceptibility, related to the proximity to half filling ($n_d = 4.8$). The effect of the non-local self-energy (not shown) is sufficiently small in this case, and does not change qualitatively (and weakly changes quantitatively) the resulting band structure (we have verified that the non-local corrections remain weak also at $\beta = 9$ eV $^{-1}$ closer to the DMFT phase transition). Although CrTe $_2$ has weak interlayer coupling and therefore represents the material for which quasi-splitting of the Fermi surface originating from magnetic correlations

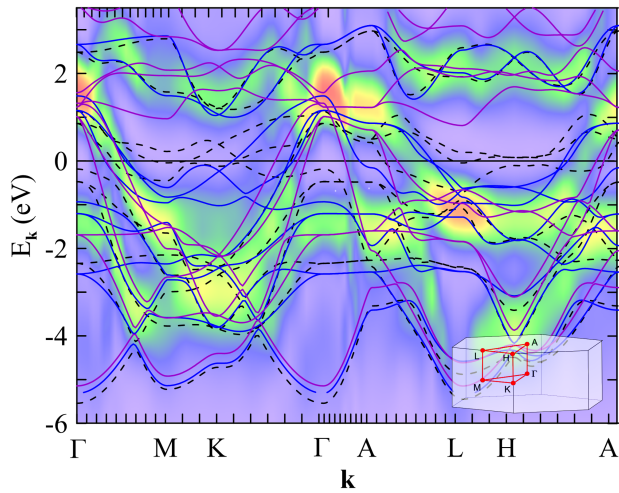


FIG. 3: (Color online) Band structure of CrTe_2 in the ferromagnetic (violet and blue solid lines for different spin projections) and non-magnetic (black dashed lines) phases, compared to the spectral density in DMFT approach

proposed previously for two-dimensional materials [8–10] could be active, we find that the effect of strong local correlations is much more pronounced due to close proximity to half filling. In view of weaker dependence of local magnetic susceptibility, than the non-local one, on temperature, we expect that band splitting in this case can be observed in a broader temperature range. Remarkably, recently the band splitting above Curie temperature was discussed for single-layer CrTe_2 , deposited on bilayer graphene [41].

Finally, we consider the electron spectral density of an altermagnet CrSb . This compound has two Cr sites per unit cell, which tend to antiferromagnetic order. Yet, these two sublattices are connected by the operation $\tilde{C}_6 = C_6\mathbf{t}$, combining the six-fold rotation C_6 with the translation $\mathbf{t} = (0, 0, c/2)$ where c is the lattice parameter along z axis. In the symmetry broken state, this yields spin splitting at $k_z \neq 0, \pi/c$ [42–45]. To visualize band structure, we choose the path, containing the points $A' = (0, 0, 4\pi/(9c))$ and $L' = 2\pi(0, 1/(\sqrt{3}a), 2/(9c))$. We use the same Coulomb interaction strength as for CrTe_2 and present the spectral functions at $\beta = 5 \text{ eV}^{-1}$ in Fig. 4, comparing them to DFT calculations in antiferromagnetic and nonmagnetic phases. The temperature in DFT+DMFT calculation is also chosen close to the Neel temperature $\beta_N = 5.9 \text{ eV}^{-1}$ ($T_N = 1950 \text{ K}$); the respective susceptibilities at the considered temperature $\chi_{\mathbf{q}=0}^{11} = 95 \text{ eV}^{-1}$ and $\chi_{\mathbf{q}=0}^{12} = -64 \text{ eV}^{-1}$ (the upper indices numerate Cr sites within the unit cell, the negative value of $\chi_{\mathbf{q}}^{12}$ indicates antiferromagnetic correlations between Cr sites belonging to the same unit cell), whose absolute values are larger than the local susceptibility $\chi_{\text{loc}} = 34 \text{ eV}^{-1}$.

One can see that both, the DFT+DMFT approach and the approach considering the non-local corrections

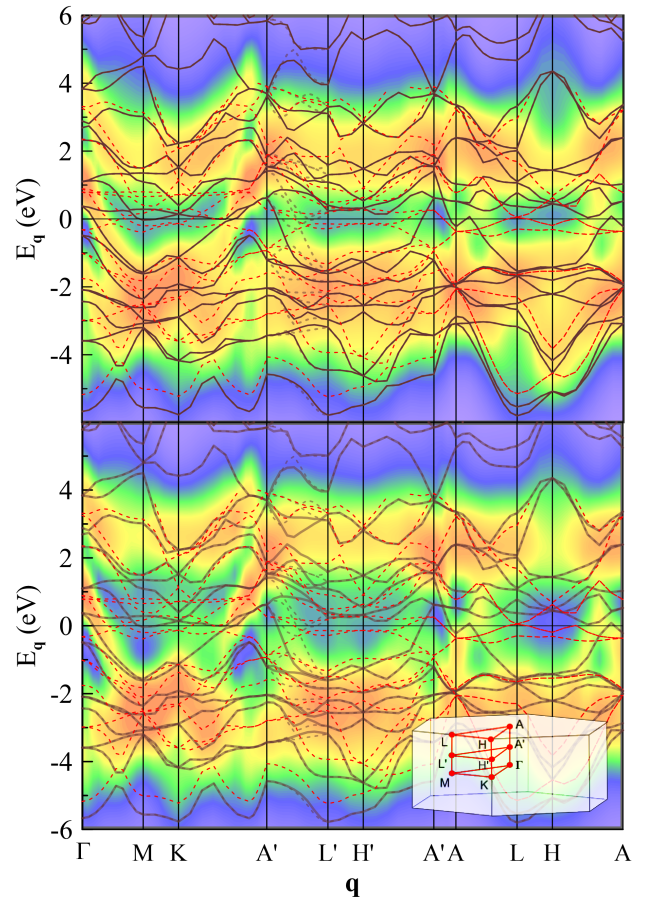


FIG. 4: (Color online) Band structure of altermagnet CrSb in the magnetic (dark solid and dashed lines for different spin projections) and non-magnetic (red dashed lines) phases, compared to the spectral density in DMFT approach (top) and the approach, accounting the non-local corrections to the self-energy (bottom) at $\beta = 5 \text{ eV}^{-1}$.

to the self-energy, lead to the splitting of the electronic spectrum of CrSb . Similarly to CrTe_2 , we attribute the large effect of local correlations to the large local susceptibility, which originates from proximity to half filling ($n_d = 4.9$). As for CrTe_2 , DFT+DMFT approach yields results quite similar to those in the ordered phase of the DFT approach. This is also pronounced in $A'-L'$ direction, where the spin splitting of the electronic spectrum is present in the DFT approach in the antiferromagnetic phase. The approach considering non-local self-energy corrections yields even larger band splitting.

In conclusion, we have analyzed the effect of the local and non-local self-energy effects on the electronic spectrum of strongly correlated itinerant magnets in the paramagnetic phase. We have obtained sufficiently strong band splitting near van Hove singularities of the electronic spectrum. For the magnets with filling of d states not very close to half filling (e. g., iron and CrO_2), we find pronounced effects of non-local magnetic correlations in the vicinity of the Curie temperature. At the same time,

for magnets with the d states filling closer to half filling (e.g. CrTe₂ and CrSb) we find strong splitting of the electronic spectrum already due to local spin correlations. Since these correlations decay slower with the increase of temperature, this effect is expected to be present in a much broader temperature range. In this respect, recent observation of band splitting in single-layer CrTe₂ [41] above the Curie temperature may be entirely due to this effect of local magnetic correlations.

The obtained split energy bands do not possess any certain spin polarization, although they each carry only part of the spectral weight of the non-magnetic bands, which brings their similarity to Hubbard subbands. However, in contrast to Hubbard subbands, they are dispersive, combining therefore itinerant and local moment features. These bands are expected to affect also transport properties (which is however the subject for separate study) due to suppression of the spectral weight at the Fermi level. We also expect that these states are highly sensitive to magnetic field. In particular, due to high magnetic susceptibility, even small magnetic fields yield strong magnetic polarization, which corresponds to having preferable spin projection of obtained bands. This may allow to control spin polarization of electronic states by weak magnetic field, without strong change of electronic

band structure, which may find its application in magnetic nano-devices and spintronics.

The considered density-density approximation overestimates the magnetic transition temperatures [16, 46, 47]. For further studies, the extension of the consideration of the present paper to the SU(2) symmetric Hund interaction is of certain interest, since it may allow one to consider magnetic transition temperatures comparable to those for experimental compounds. Also, studying the effect of self-energy and vertex corrections on the other physical observables is of certain interest.

Acknowledgements

The author is grateful to I. Dedov and I. Goremykin for discussions. Performing the DMFT calculations was supported by the Russian Science Foundation (project 24-12-00186). DFT calculations were carried out within the framework of the state assignment of the Ministry of Science and Higher Education of the Russian Federation for the IMP UB RAS. The calculations were performed on the cluster of the Laboratory of Material Computer Design of MIPT.

-
- [1] E. C. Stoner, Collective Electron Ferromagnetism, *Proc. Roy. Soc. A*, **165** (922), 372 (1938).
- [2] J. Hubbard, Electron Correlations in Narrow Energy Bands, *Proc. Roy. Soc. A* **276**, 238 (1963).
- [3] S. V. Vonsovsky, *Magnetism* (Wiley, New York, 1974).
- [4] D. C. Mattis, *The Theory of Magnetism* (Springer-Verlag, Berlin, 1981).
- [5] T. Moriya, Spin fluctuations in itinerant electron magnetism (Springer, Berlin, 1983).
- [6] K. Yosida, *Theory of Magnetism* (Springer-Verlag, Berlin, 1996).
- [7] R. M. White, *Quantum Theory of Magnetism: Magnetic Properties of Materials*, 3rd ed. (Springer-Verlag, Berlin, 2007).
- [8] A. A. Katanin, A. P. Kampf, and V. Yu. Irkhin, Anomalous self-energy and Fermi surface quasisplitting in the vicinity of a ferromagnetic instability, *Phys. Rev. B* **71**, 085105 (2005).
- [9] Y. Nomura, S. Sakai, and R. Arita, Fermi Surface Expansion above Critical Temperature in a Hund Ferromagnet, *Phys. Rev. Lett.* **128**, 206401 (2022).
- [10] M. Kitatani, Y. Nomura, S. Sakai, and R. Arita, Luttinger surface and exchange splitting induced by ferromagnetic fluctuations, *ArXiv:2509.21034*.
- [11] P. Werner, E. Gull, M. Troyer, and A. J. Millis, Spin Freezing Transition and Non-Fermi-Liquid Self-Energy in a Three-Orbital Model, *Phys. Rev. Lett.* **101**, 166405 (2008).
- [12] Z. P. Yin, K. Haule, and G. Kotliar, Kinetic frustration and the nature of the magnetic and paramagnetic states in iron pnictides and iron chalcogenides, *Nat. Mater.* **10**, 932 (2011).
- [13] L. de' Medici, J. Mravlje, and A. Georges, Janus-Faced Influence of Hund's Rule Coupling in Strongly Correlated Materials, *Phys. Rev. Lett.* **107**, 256401 (2011).
- [14] K. M. Stadler, G. Kotliar, A. Weichselbaum, J. von Delft, Hundness versus Mottness in a three-band Hubbard-Hund model: On the origin of strong correlations in Hund metals, *Annals of Physics* **405**, 365 (2019).
- [15] A. A. Katanin, A. I. Poteryaev, A. V. Efremov, A. O. Shorikov, S. L. Skornyakov, M. A. Korotin, and V. I. Anisimov, Orbital-selective formation of local moments in α -iron: First-principles route to an effective model, *Phys. Rev. B* **81**, 045117 (2010).
- [16] A. Hausoel, M. Karolak, E. Sasioglu, A. Lichtenstein, K. Held, A. Katanin, A. Toschi, and G. Sangiovanni, Local magnetic moments in iron and nickel at ambient and Earth's core conditions, *Nature Communications* **8**, 16062 (2017).
- [17] S. V. Vonsovskii, M. I. Katsnelson, and A. V. Trefilov, Localized and delocalized behaviour of electrons in metals, *Fiz. Met. Metalloved.* 76 (3) 3 (1993); 76 (4), 3 (1993).
- [18] A. Georges, G. Kotliar, W. Krauth and M. J. Rozenberg, Dynamical mean-field theory of strongly correlated fermion systems and the limit of infinite dimensions, *Rev. Mod. Phys.* **68**, 13 (1996).
- [19] V. I. Anisimov, A. I. Poteryaev, M. A. Korotin, A. O. Anokhin, and G. Kotliar, First-principles calculations of the electronic structure and spectra of strongly correlated systems: dynamical mean-field theory, *J. Phys.: Condens. Mat.* **9**, 7359 (1997).
- [20] A. I. Lichtenstein and M. I. Katsnelson, Ab initio calculations of quasiparticle band structure in correlated sys-

- tems: LDA++ approach, *Phys. Rev. B* **57**, 6884 (1998).
- [21] G. Kotliar, S. Y. Savrasov, K. Haule, V. S. Oudovenko, O. Parcollet, and C. A. Marianetti, Electronic structure calculations with dynamical mean-field theory, *Rev. Mod. Phys.* **78**, 865 (2006).
- [22] A. Toschi, G. Rohringer, A. A. Katanin, K. Held, Ab initio calculations with the dynamical vertex approximation, *Annalen der Physik*, **523**, 698 (2011)
- [23] A. Galler, P. Thunström, P. Gunacker, J. M. Tomczak, and K. Held, Ab initio dynamical vertex approximation, *Phys. Rev. B* **95**, 115107 (2017).
- [24] A. Galler, J. Kaufmann, P. Gunacker, P. Thunström, J. M. Tomczak, K. Held, Towards ab initio calculations with the dynamical vertex approximation, *J. Phys. Soc. Jpn.* **87**, 041004 (2018).
- [25] A. Toschi, A. A. Katanin, K. Held, Dynamical vertex approximation - a step beyond dynamical mean field theory, *Phys. Rev. B* **75**, 045118 (2007).
- [26] K. Held, A. A. Katanin, A. Toschi, Dynamical vertex approximation – an introduction, *Prog. Theor. Phys. Suppl.* **176**, 117 (2008)
- [27] Y. Yu, S. Isakov, E. Gull, K. Held, and F. Krien, Unambiguous fluctuation decomposition of the self-energy: pseudogap physics beyond spin fluctuations, *Phys. Rev. Lett.* **132**, 216501 (2024).
- [28] see Supplemental Material on the derivation of the non-local contribution to the self-energy and details of the temperature evolution of the spectral functions of iron.
- [29] A. A. Katanin, A. S. Belozеров, A. I. Lichtenstein, and M. I. Katsnelson, Exchange interactions in iron and nickel: DFT+DMFT study in paramagnetic phase, *Phys. Rev. B* **107**, 235118 (2023).
- [30] A. A. Katanin, Magnetic properties of half metal from the paramagnetic phase: DFT+DMFT study of exchange interactions in CrO₂, *Phys. Rev. B* **110**, 155115 (2024).
- [31] A. A. Katanin and E. M. Agapov, Magnetic properties of monolayer, multilayer, and bulk CrTe₂, *Phys. Rev. B* **111**, 035118 (2025)
- [32] P. Giannozzi, *et. al.*, Quantum ESPRESSO: a modular and open-source software project for quantum simulations of materials, *J. Phys.: Condens. Matter* **21**, 395502 (2009); Advanced capabilities for materials modelling with Quantum ESPRESSO, *ibid.* **29**, 465901 (2017); <https://www.quantum-espresso.org>.
- [33] G. Prandini, A. Marrazzo, I. E. Castelli, N. Mounet, and N. Marzari, Precision and efficiency in solid-state pseudopotential calculations, *Comput. Mater.* **4**, 72 (2018); <http://materialscloud.org/sssp>.
- [34] G. Pizzi, *et. al.*, Wannier90 as a community code: new features and applications, *J. Phys. Cond. Matt.* **32**, 165902 (2020); <http://www.wannier.org>.
The band structures are obtained using the Quantum Espresso package [32] with ultrasoft pseudopotentials from the SSSP PBEsol Precision library [33] and $16 \times 16 \times 16$ momentum grid, with subsequent Wannier projection of 3d, 4s, and 4p states with maximally localized Wannier functions, obtained within Wannier90 package [34].
- [35] M. T. Czyżyk and G. A. Sawatzky, Local-density functional and on-site correlations: The electronic structure of La₂CuO₄ and LaCuO₃, *Phys. Rev. B* **49**, 14211 (1994).
- [36] A. N. Rubtsov, V. V. Savkin, and A. I. Lichtenstein, Continuous-time quantum Monte Carlo method for fermions, *Phys. Rev. B* **72**, 035122 (2005); P. Werner, A. Comanac, L. de Medici, M. Troyer, and A. J. Millis, Continuous-Time Solver for Quantum Impurity Models, *Phys. Rev. Lett.* **97**, 076405 (2006).
- [37] Li Huang, Y. Wang, Zi Yang Meng, L. Du, P. Werner, and Xi Dai, iQIST: An open source continuous-time quantum Monte Carlo impurity solver toolkit, *Comp. Phys. Comm.* **195**, 140 (2015); Li Huang, iQIST v0.7: An open source continuous-time quantum Monte Carlo impurity solver toolkit, *Comp. Phys. Comm.* **221**, 423 (2017).
- [38] A. A. Katanin, Improved treatment of fermion-boson vertices and Bethe-Salpeter equations in nonlocal extensions of dynamical mean field theory, *Phys. Rev. B* **101**, 035110 (2020).
- [39] J. Kaufmann and K. Held, ana_cont: Python package for analytic continuation, *Comput. Phys. Commun.* **282**, 108519 (2023); https://github.com/josefkaufmann/ana_cont.
- [40] I. V. Solovyev, Linear response theories for interatomic exchange interactions, *J. Phys.: Cond. Matt.* **36** 223001 (2024).
- [41] K. Park, J.-E. Lee, D. Kim, Y. Zhong, C. Farhang, H. Lee, H. Im, W. Choi, S. Lee, S. Mun, *et. al.*, Unusual Ferromagnetic Band Evolution and High Curie Temperature in Monolayer 1T-CrTe₂ on Bilayer Graphene. *Small*, **e06671** (2025).
- [42] G. Yang, Z. Li, S. Yang, J. Li, H. Zheng, W. Zhu, Z. Pan, Y. Xu, S. Cao, W. Zhao, *et. al.*, Three-dimensional mapping of the altermagnetic spin splitting in CrSb, *Nature Communications* **16**, 1442 (2025).
- [43] M. Zeng, M.-Y. Zhu, Y.-P. Zhu, X.-R. Liu, X.-M. Ma, Y.-J. Hao, P. Liu, G. Qu, Y. Yang, Z. Jiang, *et. al.*, Observation of Spin Splitting in Room-Temperature Metallic Antiferromagnet CrSb, *Advanced Science* **11**, 2406529 (2024)
- [44] J. Ding, Z. Jiang, X. Chen, Z. Tao, Z. Liu, T. Li, J. Liu, J. Sun, J. Cheng, J. Liu, *et. al.*, *Phys. Rev. Lett.* **133**, 206401 (2024).
- [45] G. Yang, Z. Li, S. Yang, J. Li, H. Zheng, W. Zhu, Z. Pan, Y. Xu, S. Cao, W. Zhao, *et. al.*, Three-dimensional mapping of the altermagnetic spin splitting in CrSb, *Nature Communications* **16**, 1442 (2025).
- [46] V. I. Anisimov, A. S. Belozеров, A. I. Poteryaev, I. Leonov, Rotationally-Invariant Exchange Interaction: The Case of Paramagnetic Iron, *Phys. Rev. B* **86**, 035152 (2012); A. S. Belozеров, I. Leonov, V. I. Anisimov, Magnetism of iron and nickel from rotationally invariant Hirsch-Fye quantum Monte Carlo calculations, *Phys. Rev. B* **87**, 125138 (2013).
- [47] A. A. Katanin, Exchange interactions in itinerant magnets: the effects of local particle-hole irreducible vertex corrections and SU(2) symmetry of Hund interaction, *Phys. Rev. B* **112**, 085141 (2025).

SUPPLEMENTAL MATERIAL
for the paper ‘‘Splitting of electronic spectrum in paramagnetic phase of itinerant ferromagnets and altermagnets’’

1. Derivation of Eq. (3)

We consider the local interaction part of the Hamiltonian in the most general form

$$H_{\text{int}} = -\frac{1}{4} \sum_{\alpha\beta\gamma\delta} \sum_{i,mm'm''m'''} U_{\alpha\beta\gamma\delta}^{mm'm''m'''} c_{im\alpha}^+ c_{im'\beta}^+ c_{im''\gamma} c_{im'''\delta}, \quad (\text{S1})$$

where $\alpha, \beta, \gamma, \delta = \uparrow, \downarrow$ are spin indices, m, m', m'', m''' are indices of d -orbitals. The conservation of the z -component of electron spin projection together with antisymmetry $U_{\alpha\beta\gamma\delta}^{mm'm''m'''} = -U_{\alpha\beta\delta\gamma}^{mm'm''m'''}$ requires

$$U_{\alpha\beta\gamma\delta}^{mm'm''m'''} = U_{\alpha\beta}^{mm'm''m'''} \delta_{\alpha\gamma} \delta_{\beta\delta} - U_{\alpha\beta}^{mm'm''m'''} \delta_{\alpha\delta} \delta_{\beta\gamma}. \quad (\text{S2})$$

The Hamiltonian (S1) can be then reduced to

$$H_{\text{int}} = \frac{1}{2} \sum_{\alpha\beta} \sum_{i,mm'm''m'''} U_{\alpha\beta}^{mm'm''m'''} (c_{im\alpha}^+ c_{im''\alpha}) (c_{im'\beta}^+ c_{im'''\beta}). \quad (\text{S3})$$

We follow Ref. [23] of the paper and consider the equation of motion

$$\begin{aligned} [G\Sigma]_{\mathbf{k},\sigma}^{mm'}(\tau) &= \langle T c_{\mathbf{k}m\sigma}(\tau) [H_{\text{int}}, c_{\mathbf{k}m'\sigma}^+(\tau')] \rangle_{\tau' \rightarrow 0} \\ &= \sum_{\alpha} \sum_{i,mm''\tilde{m}\tilde{m}'} \sum_{\tilde{\mathbf{k}}\mathbf{q}} U_{\alpha\sigma}^{\tilde{m}\tilde{m}'m''m'} \langle T c_{\mathbf{k}\tilde{m}\alpha}^+ c_{\mathbf{k}+\mathbf{q},\tilde{m}'\sigma}^+ c_{\mathbf{k}+\mathbf{q},m''\alpha} \rangle_{\text{conn}} + \sum_{\tilde{m}} G_{\mathbf{k}\sigma}^{m\tilde{m}}(\tau) \Sigma_{\tilde{H}}^{\tilde{m}m'}, \end{aligned} \quad (\text{S4})$$

where \mathcal{T} is time ordering, conn means the connected part of the two-particle Green's function, and

$$\Sigma_H^{mm'} = \sum_{mm'\tilde{m}\tilde{m}'} \sum_{\mathbf{k}'} \left[-U_{\sigma\sigma}^{m\tilde{m},\tilde{m}'m'} \langle c_{\mathbf{k}'\tilde{m}\sigma}^+ c_{\mathbf{k}',\tilde{m}'\sigma} \rangle + \sum_{\alpha} U_{\alpha\sigma}^{\tilde{m}\tilde{m},\tilde{m}'m'} \langle c_{\mathbf{k}'\tilde{m}\alpha}^+ c_{\mathbf{k}',\tilde{m}'\alpha} \rangle \right] \quad (\text{S5})$$

is the Hartree contribution to self-energy. From the equation (S4) we find the self-energy in the form

$$\Sigma_{\mathbf{k}}^{mm'} = \Sigma_H^{mm'} + \Sigma_{F,\mathbf{k}}^{mm'},$$

where

$$\Sigma_{F,\mathbf{k}}^{mm'} = T^2 \sum_{k'q} \sum_{\alpha} F_{\sigma\alpha,kk'q}^{mm'',m'''} \tilde{m} U_{\alpha\sigma}^{\tilde{m}\tilde{m}'m''m'''} \chi_{k'q}^{0,\tilde{m}m'',\tilde{m}'m'''} G_{k+q}^{m''m'''} \quad (\text{S6})$$

and

$$\begin{aligned} F_{\alpha\beta,kk'q}^{mm',m''m'''} &= G_{k,m\tilde{m}}^{-1} G_{k'+q,m'\tilde{m}'}^{-1} G_{k+q,m''\tilde{m}''}^{-1} G_{k'm'''\tilde{m}'''}^{-1} \int d\tau_1 d\tau_2 d\tau_3 e^{i\nu\tau_1 + i(\nu'+\omega)\tau_2 - i(\nu+\omega)\tau_3} \\ &\times \langle T c_{\mathbf{k}\tilde{m}\sigma}(\tau_1) c_{\mathbf{k}+\mathbf{q},\tilde{m}'\alpha}(\tau_2) c_{\mathbf{k}+\mathbf{q},\tilde{m}''\sigma}^+(\tau_3) c_{\mathbf{k}'\tilde{m}'''\alpha}^+(0) \rangle_{\text{conn}} \end{aligned} \quad (\text{S7})$$

is the interaction vertex (here and in the following we assume summations over repeating orbital indices); $\chi_{k'q}^{0,m'm'',\tilde{m}'\tilde{m}'''} = -T G_{k'}^{m'\tilde{m}'} G_{k'+q}^{\tilde{m}''m''}$ and we have introduced frequency-momenta variables $k = (i\nu_n, \mathbf{k})$, etc. The antisymmetry of the two-particle Green's function entering Eq. (S7) yields $F_{\alpha\alpha,kk'q}^{mm',m''m'''} = -F_{\alpha\alpha,k'+q,k',k-k'}^{m'm,m''m'''} = -F_{\alpha\alpha,k,k+q,k'-k}^{mm',m''m'''} = F_{\alpha\alpha,k'+q,k+q,-q}^{m'm,m''m'''}$. We introduce

$$F_{c(s)} = -F_{\uparrow\uparrow} \mp F_{\uparrow\downarrow} \quad (\text{S8})$$

(with momenta/frequency and orbital indices omitted) and similarly for $U_{c(s)}$. This yields

$$\Sigma_{F,\mathbf{k}}^{mm'} = \frac{1}{2} T^2 \sum_{k'q} \left(F_{s,kk'q}^{mm'',m''m'''} U_s^{\tilde{m}\tilde{m}'m''m'''} + F_{c,kk'q}^{mm'',m''m'''} U_c^{\tilde{m}\tilde{m}'m''m'''} \right) G_{k+q}^{m''m'''} \chi_{k'q}^{0,m'm'',\tilde{m}'\tilde{m}''}. \quad (\text{S9})$$

In case of SU(2) symmetry $U_{\alpha\beta}$ can be chosen not depending on α, β , which yields $U_s = 0$, $U_c^{mm'm''m'''} = -2U^{mm'm''m'''}$, and the Eq. (S9) reduces to that derived in Ref. [23] of the paper. For this choice $U_{c(s)}$ do not correspond to the “true” charge and spin interaction. However, in the present paper we choose $U_{\alpha\alpha}$ antisymmetric with respect to the pairs of orbital indices (in particular, $U_{\alpha\alpha}^{mmmm}=0$), which is more convenient for Ising symmetry; the symmetric part of $U_{\alpha\alpha}$ does not give contribution to the Eq. (S6) in view of the antisymmetry of $F_{\alpha\alpha}$. In this case $U_{c(s)}$ do correspond to the interactions in charge and spin channel.

For the purposes of numerical evaluation, it is convenient to pick out the local contribution from the Eq. (S9), which together with the Hartree-Fock self-energy (S5) combines to the local self-energy $\Sigma_{\nu}^{\text{loc},mm'}$. This yields

$$\Sigma_k^{mm'} = \Sigma_{\nu}^{\text{loc},mm'} + \frac{1}{2}T^2\mathcal{N}_l \sum_{k',q} \left(F_{s,kk'q}^{mm'',m''m'} U_s^{\tilde{m}'''\tilde{m}',\tilde{m}\tilde{m}''} + F_{c,kk'q}^{mm'',m''m'} U_c^{\tilde{m}'''\tilde{m}',\tilde{m}\tilde{m}''} \right) G_{k+q}^{m'''\tilde{m}'''} \chi_{k'q}^{0,m'm'',\tilde{m}'\tilde{m}''}, \quad (\text{S10})$$

where the symbol $\mathcal{N}_{l\dots}$ takes the non-local part of the following expression. By performing the “rotation” of the channels

$$\tilde{k}' = k + q, \quad \tilde{q} = k' - k, \quad m' \leftrightarrow m''', \quad \tilde{m}' \leftrightarrow \tilde{m}''' \quad (\text{S11})$$

(such that $\tilde{k}' + \tilde{q} = k' + q$), $G_{k+q}^{m'''\tilde{m}'''} \chi_{k'q}^{0,m'm'',\tilde{m}'\tilde{m}''}$ remains unchanged. Denoting the quantities in the rotated channel by tildes (e.g. $F_{\mu} = F_{\mu,kk'q}^{mm'';m''m'}$ and $\tilde{F}_{\mu} = F_{\mu,k,k+q;k'-k}^{mm'';m'm''}$) where $\mu = \alpha\beta, c, s$, we have according to antisymmetry of $F_{\alpha\alpha}$, $\tilde{F}_{\uparrow\uparrow} = -F_{\uparrow\uparrow}$. We also denote $\tilde{F}_{\uparrow\downarrow} = F_{s\perp}$, since this vertex refers to the transverse spin channel. For SU(2) symmetry of Hund exchange the spin vertex, determined from the transverse and longitudinal channels are identical $F_{s\perp} = F_s$, but for the Ising symmetry this identity is violated. We therefore find

$$\tilde{F}_{c(s)} = \mp F_{s\perp} - \frac{F_c + F_s}{2} \quad (\text{S12})$$

and similarly for U . Therefore, the self-energy can be equivalently rewritten as

$$\Sigma_k^{mm'} = \Sigma_{\nu}^{\text{loc},mm'} + \frac{1}{2}T^2\mathcal{N}_l \sum_{k',q} \left[(F_{s,kk'q}^{mm'',m''\tilde{m}} + F_{c,kk'q}^{mm'',m''\tilde{m}}) U_{\uparrow\uparrow}^{\tilde{m}'''\tilde{m}',\tilde{m}''m'} + 2F_{s\perp,kk'q}^{mm'',m''\tilde{m}} U_{s\perp}^{\tilde{m}'''\tilde{m}',m'\tilde{m}''} \right] G_{k+q}^{m'''\tilde{m}'''} \chi_{k'q}^{0,\tilde{m}m'',\tilde{m}'\tilde{m}''}. \quad (\text{S13})$$

To derive the desired result for self-energy we, following to Ref. [27] of the paper, combine the two representations (S9) and (S13) with the weights α and $1 - \alpha$ (α is arbitrary):

$$\Sigma_k^{mm'} = \Sigma_{\nu}^{\text{loc},mm'} + \frac{1}{2}T^2\mathcal{N}_l \sum_{k',q} \left\{ \alpha (F_{s,kk'q}^{mm'',m''\tilde{m}} U_s^{\tilde{m}'''\tilde{m}',m'\tilde{m}''} + F_{c,kk'q}^{mm'',m''\tilde{m}} U_c^{\tilde{m}'''\tilde{m}',m'\tilde{m}''}) + (1 - \alpha) \left[2F_{s\perp,kk'q}^{mm'',m''\tilde{m}} U_{s\perp}^{\tilde{m}'''\tilde{m}',m'\tilde{m}''} + (F_{s,kk'q}^{mm'',m''\tilde{m}} + F_{c,kk'q}^{mm'',m''\tilde{m}}) U_{\uparrow\uparrow}^{\tilde{m}'''\tilde{m}',\tilde{m}''m'} \right] \right\} G_{k+q}^{m'''\tilde{m}'''} \chi_{k'q}^{0,\tilde{m}m'',\tilde{m}'\tilde{m}''}. \quad (\text{S14})$$

For Ising symmetry of Hund exchange, described by the Hamiltonian (2) of the main text, the orbital indexes are pairwise equal and $U_s^{mmmm} = U_0^m$ (where U_0 is the intraorbital Coulomb repulsion) and $U_s^{mm'mm'} = J^{mm'}$ (where $J^{mm'}$ is Hund interaction). At the same time, the contribution of Hund exchange is absent in the transverse channel $U_{s\perp}$ because of broken SU(2) symmetry. For correct evaluation of the transverse channel we therefore need to enforce $F_{s\perp} = F_s$ and $U_{s\perp} = U_s$. Following Refs. [23, 27] of the paper we further split the vertices into the local part and the non-local ladder contributions in the longitudinal and transverse particle-hole (ph) channels

$$F_{c(s)kk'q}^{mm'',m''\tilde{m}} = F_{c(s),\nu\nu',\omega}^{\text{loc},mm'',m''\tilde{m}} + \mathcal{F}_{c(s),\nu\nu',q}^{\text{nl},mm'',m''\tilde{m}} + \mathcal{F}_{c(s),\perp,kk'q}^{\text{nl},mm'',m''\tilde{m}}.$$

(the contribution of the particle-particle channel and multi-boson terms are assumed to be purely local). The contribution of the transverse ph channel is further expressed as a combination of “rotated” longitudinal channels according to the Eq. (S12)

$$\mathcal{F}_{s(c),\perp,kk'q}^{\text{nl}} = -\frac{1}{2}(\overline{\mathcal{F}}_{c,k,k+q,k'-k}^{\text{nl}} + \overline{\mathcal{F}}_{s,k,k+q,k'-k}^{\text{nl}}) \mp \overline{\mathcal{F}}_{s\perp,k,k+q,k'-k}^{\text{nl}}. \quad (\text{S15})$$

where the bars mark the contributions belonging to the transverse channel. We further use the identity

$$\mathcal{N}_l \sum_{k',q} F_{s(c)}^{mm'',m''\tilde{m}} G_{k+q}^{m''\tilde{m}''} \chi_{k'q}^{0,\tilde{m}m'',\tilde{m}'\tilde{m}''} = \mathcal{N}_l \sum_{k',q} \left[\mathcal{F}_{c(s),\nu\nu'q}^{mm'',m''\tilde{m}} + \mathcal{F}_{c(s),\pm,kk'q}^{mm'',m''\tilde{m}} \right] G_{k+q}^{m''\tilde{m}''} \chi_{k'q}^{0,\tilde{m}m'',\tilde{m}'\tilde{m}''} - F_{c(s),kk'q}^{\text{loc},mm'',m''\tilde{m}} G_{k+q}^{m''\tilde{m}''} \left(\chi_{k'q}^{0,\tilde{m}m'',\tilde{m}'\tilde{m}''} - \chi_{k'q}^{\text{loc},\tilde{m}m'',\tilde{m}'\tilde{m}''} \right). \quad (\text{S16})$$

In the following we neglect the contribution in the second line of Eq. (S16); we have verified that it remains sufficiently small and changes quite weakly the obtained results. Approximating again $\mathcal{F}_{s\perp} \simeq \mathcal{F}_s$ and rotating channels $\bar{\mathcal{F}}$ into \mathcal{F} according to the Eqs. (S11), we obtain

$$\Sigma_k^{mm'} = \Sigma_\nu^{\text{loc},mm'} + \frac{1}{2} T^2 \mathcal{N}_l \sum_{k',q} \left[\mathcal{F}_{c,kk'q}^{mm'',m''\tilde{m}} U_c^{\tilde{m}''\tilde{m}',m'\tilde{m}''} + 3\mathcal{F}_{s,kk'q}^{mm'',m''\tilde{m}} U_s^{\tilde{m}''\tilde{m}',m'\tilde{m}''} \right] G_{k+q}^{m''\tilde{m}''} \chi_{k'q}^{0,\tilde{m}m'',\tilde{m}'\tilde{m}''} \quad (\text{S17})$$

independently of α . Finally, using

$$T \sum_{k'} \mathcal{F}_{c(s),k,k'+q;k+q,k'}^{mm'',m''\tilde{m}} \chi_{k'q}^{0,\tilde{m}m'',\tilde{m}'\tilde{m}''} = \Gamma_{c(s),kq}^{mm'',\tilde{m}'\tilde{m}''} - 1 = \gamma_{c(s),kq}^{mm'',\tilde{m}'\tilde{m}''} [1 - U_{c(s)} \Pi_{c(s),q}]_{\tilde{m}\tilde{m}'',\tilde{m}'\tilde{m}''}^{-1} - 1 \quad (\text{S18})$$

where $\Gamma_{c(s),kq}^{mm'',m''m'''} = G_{k,m\tilde{m}}^{-1} G_{k+q,m'\tilde{m}'}^{-1} \langle c_{k\tilde{m}} c_{k+q,\tilde{m}'}^+ S_{q,m''m'''}^z \rangle_{\text{conn}}$ is the triangular vertex, $\gamma_{c(s),kq}^{mm'',m''m'''}$ is the respective reduced (Hedin) vertex, $\Pi_{c(s),q}$ is the polarization function (see, e.g., Ref. [29] for details), and introducing the effective interaction in charge (spin) channel

$$[1 - U_{c(s)} \Pi_{c(s),q}]_{\tilde{m}\tilde{m}'',\tilde{m}'\tilde{m}''}^{-1} U_{c(s)}^{m\tilde{m}',m'\tilde{m}''} = W_{c(s),q}^{m\tilde{m}',\tilde{m}'m''}, \quad (\text{S19})$$

we find

$$\Sigma_k^{mm'} = \Sigma_\nu^{\text{loc},mm'} + \frac{1}{2} T \mathcal{N}_l \sum_q \left[\gamma_{c,kq}^{mm'',\tilde{m}\tilde{m}''} W_{c,q}^{m\tilde{m}',\tilde{m}'m''} + 3\gamma_{s,kq}^{mm'',\tilde{m}\tilde{m}''} W_{s,q}^{m\tilde{m}',\tilde{m}'m''} \right] G_{k+q}^{m''\tilde{m}'}. \quad (\text{S20})$$

For pairwise equal orbital indices, considered in the density-density approximation (Eq. (2) of the main text), we obtain Eq. (3) of the main text.

2. Spectral density of iron at $\beta = 4 \text{ eV}^{-1}$

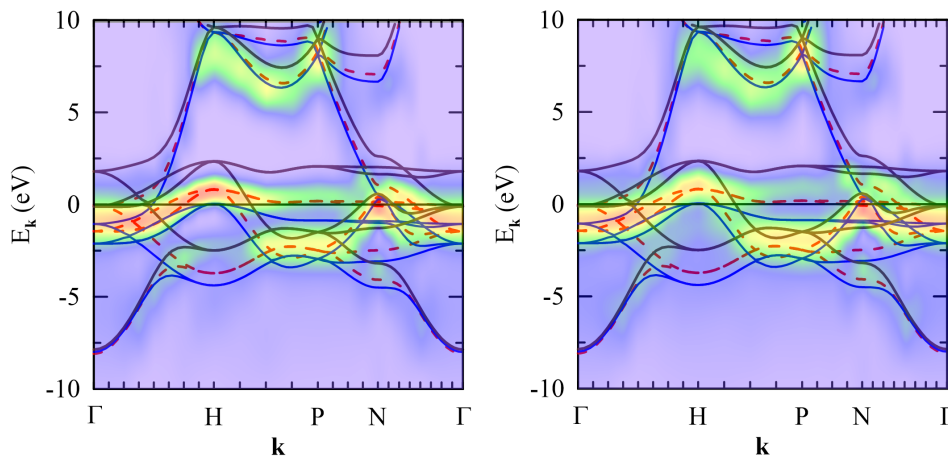


FIG. S1: (Color online) Band structure of iron in the ferromagnetic (solid lines) and non-magnetic (dashed lines) phases, compared to the spectral density in DMFT approach (left) and the approach, accounting the non-local corrections to the self-energy (right) at $\beta = 4 \text{ eV}^{-1}$. Yellow arrows show position of bands, formed by spin fluctuations in paramagnetic phase.

In this Section we present electron spectral densities (see Fig. S1) in DFT+DMFT approach and the approach considering the non-local self-energy effects at $\beta = 4 \text{ eV}^{-1}$, i.e. somewhat higher temperature, than considered in

the main text. At the considered temperature the uniform susceptibility $\chi_{\mathbf{q}=0} = 35 \text{ eV}^{-1}$ becomes only somewhat larger than the local transverse susceptibility $\chi_{\text{loc}} = 10 \text{ eV}^{-1}$. One can see that the spectral densities in DFT+DMFT approach almost did not change in comparison to that presented in Fig. 1 of the main text, while the splitting of the electronic spectrum due to non-local correlations became weaker. With further increase of temperature we therefore expect continuous approaching of the split band structure the non-magnetic one.